HHS Public Access

Author manuscript

Bone. Author manuscript; available in PMC 2023 September 26.

Published in final edited form as:

Bone. 2020 April ; 133: 115219. doi:10.1016/j.bone.2019.115219.

Biallelic variants in *KYNU* cause a multisystemic syndrome with hand hyperphalangism

Nadja Ehmke, MD[1,2,*], **Kristina Cusmano-Ozog**[3], **Rainer Koenig, MD**[4], **Manuel Holtgrewe, PhD**[5,6], **Banu Nur, MD**[7], **Ercan Mihci, MD**[7], **Holly Babcock, MS, CGC**[8], **Claudia Gonzaga-Jauregui, PhD**[9], **John D. Overton, PhD**[9], **Jing Xiao, PhD**[10], **Ariel Martinez, PhD**[11], **Max Muenke, MD**[11], **Alexander Balzer, MD**[12], **Judith Jochim, MD**[13], **Naji El Choubassi**[1,2,14], **Björn Fischer-Zirnsak, PhD**[1,2,14], **Céline Huber, PhD**[15], **Uwe Kornak, MD, PhD**[1,2,14], **Sarah Elsea, PhD**[10], **Valérie Cormier-Daire, MD, PhD**[15], **Carlos R. Ferreira, MD**[7,11,*]

[1]Charité – Universitätsmedizin Berlin, Institute of Medical Genetics and Human Genetics, Augustenburger Platz 1, 13353 Berlin, Germany

[2]Max Planck Institute for Molecular Genetics, Development and Disease Group, Ihnestr. 63-73, 14195 Berlin, Germany

[3]Biochemical Genetics and Metabolism Laboratory, Children's National Medical Center, Washington, DC 20010, USA

[4]Department of Human Genetics, University of Frankfurt, 60590 Frankfurt, Germany

[5]Core Unit Bioinformatics – CUBI, Berlin Institute of Health, Chariteplatz 1, 10117 Berlin, Germany

[6]Charité - Universitätsmedizin Berlin, Berlin 10117, Germany

[7]Department of Pediatric Genetics, Akdeniz University Medical School, 07059 Antalya, Turkey

[8]Rare Disease Institute, Children's National Health System, Washington, DC 20010, USA

[9]Regeneron Genetics Center, Regeneron Pharmaceuticals Inc. Tarrytown, NY 10599, USA

[10]Department of Molecular and Human Genetics, Baylor College of Medicine, Houston, TX 77030, USA

[*]**Correspondance to:** Nadja Ehmke, MD, Institute for Human Genetics and Medical Genetics, Charité-Universitaetsmedizin Berlin, Augustenburger Platz 1, D-13353 Berlin, Germany, nadja.ehmke@charite.de, Carlos R. Ferreira, MD, National Human Genome Research Institute, 10 Center Drive, MSC1851, Building 10, Room 9N248B, Bethesda, MD 20892, USA, carlos.ferreira@nih.gov.

Competing interest statement: Claudia Gonzaga-Jauregui is a full-time employee of the Regeneron Genetics Center from Regeneron Pharmaceuticals Inc. and receives stock options as part of compensation. All other authors declare that they have no conflict of interest.

[7]·Web Resources

FastQC: http://www.bioinformatics.babraham.ac.uk/projects/fastqc/
OMIM: https://www.omim.org/
Picard Tools: https://broadinstitute.github.io/picard/
Protein Data Bank in Europe: https://www.ebi.ac.uk/pdbe/
UniProt: https://www.uniprot.org/

[11]National Human Genome Research Institute, National Institutes of Health, Bethesda, MD 20892, USA

[12]Rahenaustr. 33, 63067 Offenbach, Germany

[13]Sana Klinikum Offenbach GmbH, Starkenburgring 66, 63069 Offenbach am Main, Germany

[14]Berlin-Brandenburg Center for Regenerative Therapies, Charité – Universitätsmedizin Berlin, Föhrerstr. 15, 13353 Berlin, Germany

[15]Department of Genetics, INSERM UMR 1163, Université Paris Descartes-Sorbonne Paris Cité, Institut Imagine, AP-HP, Hôpital Necker Enfants Malades, 75015 Paris, France

Abstract

Catel-Manzke syndrome is characterized by the combination of Pierre Robin sequence and radial deviation, shortening as well as clinodactyly of the index fingers, due to an accessory ossification center. Mutations in *TGDS* have been identified as one cause of Catel-Manzke syndrome, but cannot be found as causative in every patient with the clinical diagnosis. We performed a chromosome microarray and/or exome sequencing in three patients with hand hyperphalangism, heart defect, short stature, and mild to severe developmental delay, all of whom were initially given a clinical diagnosis of Catel-Manzke syndrome. In one patient, we detected a large deletion of exons 1–8 and the missense variant c.1282C>T (p.Arg428Trp) in *KYNU* (NM_003937.2), whereas homozygous missense variants in *KYNU* were found in the other two patients (c.989G>A (p.Arg330Gln) and c.326G>C (p.Trp109Ser)). Plasma and urine metabolomic analysis of two patients indicated a block along the tryptophan catabolic pathway and urine organic acid analysis showed excretion of xanthurenic acid. Biallelic loss-of-function mutations in *KYNU* were recently described as a cause of NAD deficiency with vertebral, cardiac, renal and limb defects; however, no hand hyperphalangism was described in those patients, and Catel-Manzke syndrome was not discussed as a differential diagnosis. In conclusion, we present unrelated patients identified with biallelic variants in *KYNU* leading to kynureninase deficiency and xanthurenic aciduria as a very likely cause of their hyperphalangism, heart defect, short stature, and developmental delay. We suggest performance of urine organic acid analysis in patients with suspected Catel-Manzke syndrome, particularly in those with cardiac or vertebral defects or without mutations in *TGDS*.

Keywords

Skeletal dysplasia; hyperphalangism; Catel-Manzke syndrome; KYNU; kynureninase deficiency; xanthurenic aciduria

1. Introduction

Catel-Manzke syndrome (MIM 616145) is characterized by the combination of Pierre Robin sequence (microretrognathia, cleft palate and glossoptosis) and a unique hand malformation, referred to as Manzke dysostosis, i.e., the presence of an accessory ossification center between the second metacarpal and proximal phalanx, leading to shortening, radial deviation and clinodactyly of the index fingers [1, 2]. Additional features include congenital heart defects, short stature, pectus deformities, and clubfoot [3]. Recently, we identified biallelic

mutations in *TGDS* (MIM 616146) in patients with Catel-Manzke syndrome as well as in a fetus with additional shortening of the middle fingers, suggesting that mutations in this gene may cause a broader phenotypic spectrum [4, 5]. Still, the molecular etiology in several cases remains unknown [6, 7].

The aim of this study is to identify additional genes related to Catel-Manzke syndrome. We describe three unrelated patients diagnosed with Catel-Manzke syndrome with biallelic mutations in *KYNU* (MIM 605197), encoding kynureninase (EC 3.7.1.3), an enzyme in the tryptophan catabolic pathway necessary for the biosynthesis of nicotinamide adenine dinucleotide (NAD^+), a cofactor important for enzymatic reactions across multiple biochemical pathways. Biallelic loss-of-function (LOF) mutations in *KYNU* and *HAAO* (a gene encoding 3-hydroxyanthranilate 3,4-dioxygenase, an enzyme immediately distal to kynureninase in the tryptophan catabolic pathway) have recently been described as the cause of a complex malformation syndrome, namely Vertebral, Cardiac, Renal, and Limb defects syndrome type 2 and 1, respectively (VCRL1, MIM #617660 and VCRL2, MIM #617661), in four unrelated patients [8]. Two siblings with kynureninase deficiency exhibiting abnormal concentrations of metabolites along the tryptophan catabolic pathway but with no reported congenital malformations were also previously reported [9]. We describe for the first time the presence of microretrognathia and hyperphalangism, cardinal signs of Catel-Manzke syndrome, in the setting of kynureninase deficiency.

2. Clinical reports

Patient 1 is a 13-year-old male of Caribbean descent. Family history was unremarkable. He was born at 36 weeks of gestation after an uncomplicated pregnancy and delivery with a birth weight of 2900 g (−2.16 SD). His exact birth length was not recalled, but was reportedly normal. Hypoplastic left heart syndrome was diagnosed shortly after delivery and a Fontan procedure was subsequently performed. Short stature became a concern at 2 years of age. He was noted since early childhood to have radial deviation and clinodactyly of the index fingers (Figure 1C), for which hand X-rays were eventually obtained. This imaging revealed a supernumerary epiphyseal center located on the ulnar side of the base of the proximal phalanx of the index finger bilaterally (Figure 1D). Therefore, he was clinically diagnosed with Catel-Manzke syndrome at 10 years of age. He had a history of delayed motor and speech development, with achievement of independent walking and first words at 2 years of age. He received occupational therapy, physical therapy, adaptive therapy and speech therapy for a few years, and his academics are still supported by an individualized education program. A formal neurodevelopmental evaluation excluded cognitive delay; in fact, the Wide Range Achievement Test version 4 (WRAT-4, blue form) administered at the age of 8 years yielded a raw score of 32 in math and a raw score of 57 in word reading, placing him above his grade level. He was toilet trained to stool at 7 years of age, and had severe behavioral problems warranting a formal diagnosis of attention deficit hyperactivity disorder (ADHD) at 8 years of age. At 13 years and 3 months, he developed symptomatic bradycardia due to a third-degree atrioventricular (AV) block, necessitating a pacemaker implant. There were no clinical signs of hearing impairment. Recent measurements show a height of 139.7 cm (−2.4 SD, average for a 10-year-old boy), weight of 52.3 kg (+0.51 SD) and head circumference (HC) of 52.8 cm (−1.50 SD). He has highly arched eyebrows

(Figure 1A), microretrognathia with high palate (Figures 1B, 1E), butterfly vertebrae at T10-T11 with scoliosis (Figure 1K), and hepatomegaly from congestion. No variants in genes previously associated with hyperphalangism (*TGDS, IMPAD1*, *CANT1, CHSY1* or *ERF*) were identified.

Patient 2 is a 3-year-old female who was born at term as the first child of healthy, consanguineous parents of Turkish descent. Family history was unremarkable. Pregnancy was complicated by a prenatal diagnosis of tetralogy of Fallot. Her birth weight was 2970 g (−0.7 SD), length 49 cm (−0.9 SD) and HC 35 cm (+0.08 SD). At birth, radial deviation and clinodactyly of both index fingers was noted, due to supernumerary ossicles at the base of the second basal phalanges (Figure 1H, I). Therefore, a diagnosis of Catel-Manzke syndrome was given postnatally, although she did not have appreciable Pierre Robin sequence. She also had long thumbs and butterfly vertebrae at T8 (Figure 1P). Surgical correction of her heart defect was performed at the age of 7 months. During the intervention there was left ventricular decompensation due to a previously undiagnosed anomalous origin of the left coronary artery from the pulmonary artery (ALCAPA). After this episode she required extracorporeal membrane oxygenation (ECMO) for two weeks, and needed a pacemaker. She presented with severe muscular hypotonia and loss of all achieved developmental milestones. Feeding difficulties required the placement of a percutaneous endoscopic gastrostomy (PEG) tube at the age of 8 months. An EEG at the age of 9 months showed multifocal seizure-typical activity, which was suspected to derive from hypoxia during left ventricular decompensation. First seizures occurred at the age of 12 months (abnormal eye and hand movements). Later, EEG showed bilateral sharp waves/spike waves and she presented with tonic seizures and atypical absence seizures, therefore Lenox-Gaustaut syndrome was diagnosed. Under treatment with valproate and levetiracetam, EEG abnormalities and seizures improved significantly. Brainstem evoked response audiometry (BERA) at the age of 1.5 years revealed sensorineural hearing loss (right side: severe, left side: mild). A cranial CT scan showed an incomplete partition type II of the right cochlea as well as hypoplasia of the left cochlea, a malformed left horizontal semicircular canal with cystic fusion with the vestibular duct, and a dilated left posterior semicircular canal. When last seen at the age of 3 years 7 months, there was severe developmental delay, short stature and microcephaly. She could roll over as well as grab and hold things but did not sit unsupported, stand or crawl, and remained non-verbal. Her height was 81.5 cm (−4.7 SD), weight 10.6 kg (−0.64 SD) and HC 43.3 cm (−6.4 SD). She had a low anterior hairline, thick scalp hair, narrow forehead, and full cheeks (Figure 1F, G). Her chin and palate were normal. Chromosomal analysis after amniocentesis showed a normal karyotype 46,XX. Postnatally, no mutations in *TGDS* were identified.

Patient 3 is a 10-year-old female, first referred to clinic for dysmorphic facial features and hand malformations at the age of 2 years. Pregnancy was complicated by an abnormal triple screen test; amniocentesis was performed, and chromosome analysis revealed a normal 46,XX karyotype. She was born at term by vaginal delivery as the second living child of healthy consanguineous parents of Turkish descent. Apgar scores were normal. Her birth weight was 2400 g (−1.9 SD), length 48 cm (−1.4 SD), and HC 34 cm (−0.2 SD). Radial deviation and clinodactyly of both index fingers, as well as short middle

fingers, were noted at birth (Figure 1N). A Catel-Manzke syndrome diagnosis was given at the age of two years. She had joint laxity, with particularly hyperextensible knees. Her motor development was normal. However, a neurodevelopmental evaluation at 5 years of age diagnosed mild cognitive delay and learning difficulties. Echocardiogram detected a secundum atrial septal defect, and a subaortic ventricular septal defect (VSD). Agenesis of the right kidney was observed on renal ultrasound. Hand radiographs at the age of 5 years showed several abnormalities, as shown in Figure 1O. In addition to Manzke dysostosis, there were longitudinal epiphyseal brackets at the base of the third proximal phalanges and at the second metacarpals. Additional features noted on physical examination included a flat face, high anterior hairline, prominent forehead, depressed nasal bridge, narrow mouth with thin vermilion of her upper and lower lips and downturned corners of the mouth, high palate, microretrognathia, as well as low-set and protruding ears (Figure 1L). There were no clinical signs of hearing impairment. At 4 years and 10 months, her height was 98 cm (−2.2 SD), her weight 17 kg (+1.3 SD) and her HC 47.2cm (−2.3 SD). The family history was significant for two previous spontaneous abortions from the patient's parents as well as a third pregnancy resulting in stillbirth at term. This stillborn female had similar clinical findings to the proband, including dysmorphic facial features and hand anomalies.

The most important clinical features of the patients are summarized in Table 1.

3. Material and Methods

3.1 Ethics approval

The study was approved by the ethics committee of the Charité – Universitätsmedizin Berlin, the Institutional Review Board at Children's National Medical Center, and by the ethics committee of the Necker Hospital (Paris). All procedures followed were in accordance with the ethical standards of the responsible committee on human experimentation (institutional and national) and with the Helsinki Declaration of 1975, as revised in 2000. Informed consent was obtained from all patients included in the study. Additional informed consent was obtained from all patients for whom identifying information is included in this article.

3.2 Human material

Venous blood and urine samples were obtained from the patients by standard procedures. Genomic DNA was extracted from peripheral blood leukocytes using standard protocols.

3.3 Microarray-based comparative genomic hybridization (array CGH)

Copy number analysis was performed according to manufacturer's guidelines using the CytoScan™ XON Suite microarray platform (Thermo Fisher Scientific), an exon-level copy number assay with enhanced coverage in ~7000 clinically relevant genes and ~19,000 other genes and intergenic regions, thus providing whole-genome coverage. The CytoScan XON microarray consists of 6.85 million probes, including 6.5 million copy-number probes and 300,000 single-nucleotide polymorphism (SNP) probes that allow for sample tracking, duo/trio analysis, and loss of heterozygosity (LOH) analysis. Cel files were processed in the

Chromosome Analysis Suite v 3.3 software (Thermo Fisher Scientific) and the genes were filtered by level of significance for analysis and reporting.

3.4 Exome sequencing and analysis

Exome sequencing of Patient 1 and his mother was performed in collaboration with the Regeneron Genetics Center (RGC). Briefly, the IDT XGen exome capture reagent was used for target enrichment of DNA samples. Sequencing was performed on an Illumina HiSeq 2500 sequencer using v4 chemistry. After sequencing, the data was processed through a cloud-based pipeline developed at the RGC that runs standard mapping and alignment bioinformatics tools. Data were generated and de-multiplexed using Illumina's CASAVA software. Sequence reads were mapped and aligned to the GRCh38 human genome reference assembly using BWA-MEM [10]. Duplicate reads were marked and flagged using Picard tools and indels were realigned using GATK [11] to improve variant call quality. SNP and INDEL variants and genotypes were called using GATK's HaplotypeCaller to generate sample specific variant calling files. Called variants were analyzed using an RGC implemented bioinformatics analysis pipeline as previously described [12]. Variants were classified and annotated based on their potential functional effects using RefSeq and ENSEMBL75 transcripts. Algorithms for bioinformatic prediction of functional effects of variants, such as Polyphen2 [13] (HumVar scores, cutoff ≥0.447), SIFT [14] (cutoff ≤0.05), and MutationTaster [15] (cutoff: qualitative prediction as pathogenic), along with conservation scores based on multiple species alignments were incorporated as part of the annotation process. Variants were subsequently filtered based on their observed frequencies in population control databases such as dbSNP [16], the 1000 Genomes Project [17], the Exome Aggregation Consortium Database (ExAc) [18], and the internal RGC database in order to filter out common polymorphisms and high frequency, likely benign variants. Rare variants below a 1% minor allele frequency (MAF) threshold were considered for downstream analysis. We annotated passing variants according to the genotypes observed in the available maternal sample and to impute paternal variants. If the variants were present in the mother these were considered 'maternally inherited', variants with a minor allele count (MAC) >1 not present in the maternal sample were considered 'putative paternally inherited', whereas variants with MAC <1 were considered 'possible *de novo*' variants. Given the absence of the paternal sample for this family, we compared the proband's genotypes and the maternal genotypes to infer the paternal genotypes. This allowed us to identify all potential candidate variants in genes of interest that fulfill Mendelian expectations for an affected male child with reportedly unaffected parents including homozygous recessive, compound heterozygous, X-linked recessive, and potential *de novo* variants. Additional targeted exome analysis was performed to look for coding variants of interest in *KYNU* that were predicted deleterious and not maternally inherited.

Illumina's All Exon Kit V6 was used for targeted enrichment of DNA of Patient 2 and her parents. The reads were aligned using BWA-MEM v0.7.15 to the reference GRCh37 (hs37d5.fa), separate read groups were assigned for all reads from one lane, and duplicates were masked using Samblaster v0.1.24 [19]. Standard QC was performed using FastQC. The variants were called using GATK UnifiedGenotyper v3.7 and annotated with Jannovar v0.24 [20] using RefSeq v105 exons, ExAC v0.3.1 and gnomAD v2.0.1, dbSNP and COSMIC

v72 [21]. The following filters were applied for obtaining a list of variants of interest. We excluded variants that were seen in homozygous state in ExAC, seen in any population in ExAC or gnomAD [22] above 1%, those flagged in COSMIC or dbSNP as common (to remove common artifacts resulting from differences between our pipeline and the one of ExAC/gnomAD). We further excluded variants that were functionally flagged as intergenic, upstream/downstream, within the UTR, only had an effect on non-coding transcripts, those in intronic regions, and those predicted to have no stronger effect than synonymous base exchange. We kept variants annotated as potentially affecting splicing. The remaining variants were filtered according to an autosomal dominant and autosomal recessive mode of inheritance. Parenthood was confirmed using the algorithm Peddy [23].

For Patient 3, exome capture was performed at the genomic platform of the IMAGINE Institute (Paris, France) with the SureSelect Human All Exon v4 kit (Agilent Technologies). The library was prepared from 3 μg of genomic DNA sheared with Ultrasonicator (Covaris) as recommended by the manufacturer. Barcoded exome libraries were pooled and sequenced using the HiSeq2500 system (Illumina), generating paired-end reads. After demultiplexing, sequences were mapped onto the human genome reference (NCBI build37/hg19) with BWA. The mean depth of coverage obtained for each sample was ≥ x80 with 95% of the exome covered at minimum at 15x. Variant calling was carried out with GATK, SAMtools [24] and Picard Tools. Single nucleotide variants were called with GATK UnifiedGenotyper, whereas indel calls were made with the GATK IndelGenotyper v2. All variants with a read coverage ≤x2 and a Phred-scaled quality of ≤20 were filtered out. All the variants were annotated and filtered using an in-house developed annotation software system (Polyweb, unpublished). The first round of analysis focused on non-synonymous variants, splice variants, and coding indels. The potential pathogenicity of variants was evaluated using SIFT, PolyPhen2 and MutationTaster prediction algorithms. The frequency in control populations was evaluated using the ExAC database, dbSNP, and the 1000 Genomes Project; other datasets such as ClinVar [25] and in-house exome data were also assessed. The detected *KYNU* variants were tested in the parents using Sanger sequencing.

3.5 Urine organic acid analysis

Urine was prepared by first adding the internal standard, 3,4-dimethoxyphenylacetic acid, followed by an ethyl acetate extraction, then dried at 50 °C in a water bath under nitrogen. The dried extract was then derivatized by silylation with N,O-bis-(trimethylsilyl)trifluroacetamide containing trimethylchlorosilane (BSTFA + 10% TMCS), and separated on a J&W DB-5ms GC phenyl arylene polymer capillary column, 25 m, 0.20 mm, 0.33 μm, 7-inch cage, purchased from Agilent Technologies, catalog #128–5522. The chromatograph was obtained in full scan mode using a Hewlett-Packard 7890 gas chromatograph coupled with a 5975C mass selective detector. The gas chromatograph and mass spectrometer were interfaced with a Hewlett-Packard/Microsoft Windows 95 computer system. The retention times of organic acids on the Total Ion Chromatogram (TIC) were based on the oven temperature ramp that is programmed from 80 to 315°C at a variable incline each minute. Xanthurenic acid was identified by retention time (30.84 minutes) and fragmentation pattern (ions = 406, 420). Of note, the sample from Patient 2 was extracted from a dried urine spot.

3.6 Global metabolomics

Metabolomic profiling of small molecules (75–1000 Da) was performed by Baylor Genetics (Houston, TX) and Metabolon, Inc. (Durham, NC), as described previously [26–29]. Briefly, plasma was collected in EDTA-containing tubes, isolated by centrifugation, and kept frozen until analysis; urine was immediately frozen. Both plasma and urine samples were thawed on ice before extraction. Small molecules were extracted in an 80% methanol solution before being analyzed by four different mass spectrometry methods. The first method utilized acidic, positive ionization conditions chromatographically optimized for hydrophilic compounds (UPLC-MS/MS Pos polar). The second method used the same acidic positive ionization conditions but was chromatographically optimized for hydrophobic compounds (UPLC-MS/MS Pos lipid). The third method used negative ionization optimized conditions (UPLC-MS/MS Neg), and the final method utilized negative ionization optimized conditions with hydrophilic interaction liquid chromatography (UPLC-MS/MS Polar). All chromatographic separations were completed using an ACQUITY UPLC (Waters) equipped with either a Waters BEH C18 or Waters BEH Amide column followed by analysis with an Orbitrap Elite high-resolution mass spectrometer (Thermo-Finnigan). The chemical structures of known metabolites were identified by matching the ions' chromatographic retention index, nominal mass, and mass spectral fragmentation signatures with reference library entries created from authentic standard metabolites under the identical analytical procedure as the experimental samples. Currently, the reference library contains entries for ~2500 unique human metabolites. Semi-quantitative analysis was achieved by comparing patient samples to a set of invariant anchor specimens. Raw spectral intensity values were normalized to the anchor samples, log transformed, and compared to a normal reference population to generate Z-score values. Median raw intensity values were calculated for all analytes identified in ≥2/3 of the anchor specimens, and these median values were then used to normalize corresponding analyte raw intensity values in the patient specimen. Analytes not identified in at least 2/3 of the anchor specimens were excluded from analysis or were identified as rare molecules, if identified in <5% of cohort samples. Z-scores were calculated using the mean and standard deviation of the entire median-scaled log-transformed dataset.

3.7 Statistics

To compare the control and patient groups, unpaired Student's t-tests were used to identify informative biomarkers, where a two-tailed p-value <0.05 was considered statistically significant. Receiver Operating Characteristic (ROC) curve analysis was performed to calculate sensitivity and specificity, with the Youden index used for selection of the best Z-score cutoff. Statistical analysis was performed with Prism version 6.0c (Graphpad Software Inc, La Jolla, CA). Statistical figures were also designed with Prism; the solid line represents the mean, while top and bottom lines represent standard errors of the mean.

4. Results

4.1 Genomic findings

In Patient 1, array CGH showed an 85 kb deletion of 2p22.2 (arr[GRCh37]2q22.2(143,634,577–143,719,262)x1), including exons 1–8 out of 14 exons of

KYNU (NM_003937.2; exons 1–9 in transcript NM_001199241.1) (Figure 2, Supplemental Figure 1A), which was maternally inherited (Supplemental Figure 1B). Targeted analysis of the exome data of this patient for rare, potentially deleterious, and not maternally-inherited variants in *KYNU* revealed the missense variant c.1282C>T (p.Arg428Trp) in exon 14 (chr2[GRCh37]:g.143799625C>T, rs147475752). The variant is not present in the mother and therefore was assigned to be "putatively paternally-inherited" in the analysis (Figure 2, Supplemental Figure 1C). The father was not available for sequencing or confirmation, due to accidental demise. Given that the mother is not a carrier of the identified missense variant and that this has been previously reported in population databases (gnomAD MAF= 0.007%; 18 heterozygotes), the most likely explanation is that the proband inherited this variant from his father. However, given the unavailability of a paternal sample, we cannot discard the possibility of the variant to be a recurrent *de novo* mutation in the proband. No rare variants in genes previously associated with hyperphalangism were identified.

Trio exome sequencing of Patient 2 and her parents revealed the homozygous missense variant c.989G>A (p.Arg330Gln) in exon 12 of *KYNU* (chr2[GRCh37]:g.143790838G>A, rs142934146) in the proband when filtering according to the autosomal recessive model of inheritance (Figure 2, Supplemental Figure 1D). No *de novo* variants and no rare variants in genes previously associated with hyperphalangism were identified. We also detected a homozygous missense variant c.1171C>G (p.Pro391Ala; chr16[GRCh37]:g.21262058C>G) in exon 2 of *ANKS4B* (NM_145865.2, MIM 609901) in the proband, affecting a highly conserved amino acid position and present in a heterozygous state in six individuals in the gnomAD browser (minor allele frequency 0.002%). Mutations in *ANKS4B* are not currently reported in association with any known diseases.

Exome sequencing of Patient 3 showed the homozygous missense variant c.326G>C (p.Trp109Ser) in exon 4 of *KYNU* (chr2[GRCh37]:g.143685263G>C, rs780720490). Sanger sequencing confirmed biparental inheritance. No rare variants in genes previously associated with hyperphalangism were identified.

The gnomAD browser shows that the missense variant c.1282C>T in *KYNU* is present in a heterozygous state in 18 individuals, the variant c.989G>A in one individual and the variant c.326G>C in three, for a minor allele frequency of 0.007%, 0.0004%, and 0.0008%, respectively. No individuals have been reported to date to be homozygous for these variants in any available database. All *KYNU* variants were classified as disease-causing by MutationTaster and probably damaging by PolyPhen-2 as a result of the evolutionary conservation of the amino acids at positions 428, 330 and 109 (Figure 2), whereas only p.Arg428Trp and p.Trp109Ser were classified as deleterious by SIFT. The CADD PHRED score v1.4 of c.1282C>T is 23.3, of c.989G>A 25.7 and of c.326G>C 29.9 [30]. According to the kynureninase crystal structure 3E9K deposit in EMBL-MBI all affected residues reside within secondary structure elements (KYNU_HUMAN, Q16719). In case of Trp109 and Arg330 the substitutions might affect the formation of alpha helices whereas the substitution on Arg428 could affect a beta sheet. These potential alteration in secondary structure might cause changes in the 3D conformation and thereby enzymatic dysfunction. Although variants in *KYNU* were previously associated with multiple malformations [8]

and altered tryptophan metabolism [9], they were not previously associated with Manzke dysostosis or other forms of hyperphalangism.

4.2 Biochemical findings

Metabolomics analysis of urine and plasma of patients 1 and 2 revealed highly statistically significant elevations of urine 3-hydroxykynurenine (Z-score Patient 1: +8.89, Patient 2: +7.17; mean: +8.03), urine xanthurenate (Z-score Patient 1: +7.06, Patient 2: +4.62; mean: +5.84), and plasma xanthurenate (Z-score Patient 1: +8.72, Patient 2: +6.36; mean: +7.54), with highly statistically significant decreases in urine picolinate (Z-score Patient 1: −4.08, Patient 2: −3.55; mean: −3.81) and urine quinolinate (Z-score Patient 1: −8.46, Patient 2: −2.03; mean: −5.25) (Table 2, Figure 3). Thus, there was an increase in analytes proximal to the metabolic block, with a decrease in metabolites distal to the block along the tryptophan catabolic pathway (Figure 4), as expected. ROC curve analysis revealed ideal Z-score cutoff values of different metabolites for discrimination between controls and patients with kynureninase deficiency (Supplemental Table 1). A urine 3-hydroxykynurenine Z-score >4.89, urine xanthurenate Z-score >3.86, plasma xanthurenate Z-score >5.04, and urine picolinate <−3.45 using our clinically-available metabolomics platform is supportive of kynureninase deficiency. In addition, we performed organic acid analysis on urine samples obtained from two of three patients. Xanthurenic acid was present in both urine samples, though levels were significantly higher in Patient 1 (Supplemental Figures 2 and 3). Using the same method, xanthurenic acid was not identified in healthy controls or samples from others with known inborn errors (n=10) and was also not identified in a heterozygous deletion carrier (mother of Patient 1). Plasma and urine samples could not be obtained for Patient 3.

5. Discussion

Although congenital anomalies were previously described in the setting of kynureninase deficiency, we report for the first time the combination of cardinal findings of Catel-Manzke syndrome, such as microretrognathia and hyperphalangism. We detected likely LOF or hypomorphic variants including a deletion (exons 1–8) and three very rare missense variants in *KYNU* in three unrelated individuals who had previously received a clinical diagnosis of Catel-Manzke syndrome. The multiexonic deletion in *KYNU* likely represents a LOF variant. The variants were either confirmed or presumed to be biallelic in all patients. Only Patient 1 lacked confirmation due to the absence of paternal evaluation; therefore, *de novo* occurrence of the second variant in *cis* cannot be excluded. Given the discovery of homozygous missense variants in two unrelated patients and the phenotypic overlap of all patients, biallelic status of the variants in Patient 1 seems highly likely.

The pattern of malformations in our patients–including short stature, vertebral malformations (in Patient 1), inner ear malformations (in Patient 2) and congenital heart and renal defects–significantly overlaps with VCRL1 and VCRL2. Our patients also present with the addition of the cardinal feature of Catel-Manzke syndrome, hand hyperphalangism, which was not described in the patients reported with VCRL1 or VCRL2. Another typical manifestation of the syndrome, namely microretrognathia, was also previously unreported,

but was present in two individuals in our cohort. In contrast to the four previously reported patients with VCRL1 and VCRL2, all of our patients had at least one missense variant in *KYNU*, as opposed to truncating variants, which could explain the phenotypic differences. Our findings may explain another portion of *TGDS*-negative Catel-Manzke syndrome, and suggest a possible genotype-phenotype correlation in patients with kynureninase deficiency. Figure 2 shows an overview of all reported *KYNU* mutations. Table 1 summarizes the mutation and clinical data of our cohort compared to the patients previously reported with VRCL1 and VCRL2 and patients with *TGDS* mutations. Unlike patients with *TGDS* mutations, our patients had developmental delay, although the severe developmental delay, muscular hypotonia and seizures of Patient 2 could be explained by cardiac decompensation requiring ECMO during the two weeks after her cardiac surgery. Additionally, the type of heart defects in two patients of our cohort (hypoplastic left heart, tetralogy of Fallot) is more severe than that reported in individuals with *TGDS* mutations. It is unclear whether the severe microcephaly of Patient 2 is caused by the *KYNU* mutation. The two patients reported with *HAAO* mutations had microcephaly but in the mild range [8].

Metabolomics analysis of urine and plasma of patients 1 and 2 are supportive of kynureninase deficiency and therefore of a pathogenic effect of the detected *KYNU* variants. There was an increase in analytes proximal to the metabolic block, with a decrease in metabolites distal to the block along the tryptophan catabolic pathway (Figure 4). Elevations of 3-hydroxykynurenine, kynurenine and xanthurenate with a normal tryptophan concentration were previously reported in the setting of kynureninase deficiency [8, 9], while we demonstrate for the first time a decrease in 3-hydroxyanthranilate, picolinate, and quinolinate in this condition. Additionally, we found xanthurenic aciduria in both patients on urine organic acid analysis. Christensen *et al.* found a missense variant leading to the amino acid substitution p.Thr198Ala in two brothers with significant hydroxykynureninuria and xanthurenic aciduria but without congenital malformations [9]. The *in vitro* results of Shi *et al.* indicate that this amino acid substitution is associated with significant residual activity (64%), which may explain the absence of congenital malformations in the two brothers [8]. This illustrates that the amount of xanthurenic acid excretion might depend on different factors and does not necessarily correlate with the development or severity of congenital malformations, but still indicates reduced kynureninase activity. Our results demonstrate that the detection of xanthurenic aciduria on organic acid analysis, a readily available assay, could be used as a tool to narrow the differential diagnosis of patients with skeletal dysplasia including hyperphalangism.

Niacin, or vitamin B3, is a term collectively applied to nicotinic acid and nicotinamide, both serving as sources of NAD^+ [31]. Dietary tryptophan is considered a niacin equivalent, as 1 mg of niacin is obtained from 60 mg of tryptophan [32]. Postnatally, about half of the niacin equivalent intake is derived from tryptophan [33], so the more severe the metabolic block, the less NAD^+ available. Milder blocks in the tryptophan degradation/niacin synthesis pathway lead only to xanthurenic aciduria, while more severe blocks in NAD^+ synthesis will lead to congenital malformations due to the deficiency of multiple NAD^+-dependent enzymes. It should be noted that even patients with clinical pellagra from niacin deficiency could have normal levels of urinary niacin metabolites and whole blood NAD^+ [34]. In addition, the paper by Shi et al. [8] reported the concentration of metabolites along the

kynurenine pathway in one patient with kynurenine deficiency, and found a 9-fold decrease in NAD^+ relative to two unaffected family members, as compared to a 161-fold increase in 3-hydroxykynurenine. The same paper revealed that in an animal model of kynureninase deficiency, the adult mutant mouse has normal NAD^+ concentrations in serum, while 3-hydroxykynurenine is markedly abnormal. Thus, measurements of NAD^+ concentrations in blood might not represent a sensitive marker of NAD^+ deficiency, while measurement of other metabolites along the kynurenine pathway are much more markedly abnormal than NAD^+ concentrations. At present, it remains unclear if niacin supplementation could improve the developmental and behavioral phenotype seen in our patients, or if individuals with kynureninase deficiency could be at risk of developing pellagra.

It is remarkable that most disorders associated with an accessory phalangeal ossification center, or hyperphalangism, are likely related to abnormal glycosaminoglycan (GAG) synthesis. Figure 4 summarizes the known causes of hyperphalangism due to defects in the biosynthetic pathway of chondroitin sulfate, one of the most common glycosaminoglycans in cartilage [35]. *TGDS* encodes TDP-glucose 4,6-dehydratase, an enzyme that participates in the synthesis of rhamnose in bacteria and plants. It is unknown how this enzyme functions in mammals, as rhamnose is not known to be present in this class. Its closest paralog is *UXS1* [4], which encodes UDP-xylose synthase (also known as UDP-glucuronate decarboxylase) that decarboxylates UDP-glucuronic acid to UDP-xylose in the Golgi. This UDP-xylose is then used as a substrate for the synthesis of the linker tetrasaccharide that serves as an anchor for the attachment of glycosaminoglycans to proteoglycans [36]. It should be noted that both *TGDS* and *UXS1* are expressed in chondrocytes [37] (see Supplemental Figure 4), and both are NAD^+-dependent enzymes. Thus, a deficiency of kynureninase could impair their function, due to lack of synthesis of their cofactor. The assumed different phenotypic effects of complete LOF and missense variants could be related to the extent of NAD^+ deficiency in specific stages during embryonic development. Although we focus specifically on the hypothetical mechanism for hyperphalangism in the setting of kynureninase deficiency, it should be noted that NAD^+ is a cofactor for hundreds of enzymatic reactions, and thus many processes are likely to be disrupted and lead to the multiple clinical issues found in affected individuals.

A special mention should be made of the hand defects in Patient 3, who in addition to hyperphalangism of the index fingers also had segmentation of the second metacarpals. Short stature, micrognathia, palatal defects, developmental delay, radial deviation of the index fingers, and a segmented second metacarpal are features described in patients with Devriendt syndrome [38–40]. Thus, genes encoding enzymes in the tryptophan catabolism pathway may represent potential candidates for this rare syndrome.

In conclusion, our results contribute to the elucidation of the genetic etiologies of phenotypes resembling Catel-Manzke syndrome and might uncover a new genotype-phenotype correlation. Further functional studies are needed to confirm the deleterious effect on kynureninase activity of the identified variants and their specific impact on phalangeal bone formation.

Supplementary Material

Refer to Web version on PubMed Central for supplementary material.

Acknowledgements

The authors wish to thank the patients and their families for their cooperation and support, as well as Theresa Wilson, Gabriele Hildebrand and Julie Huppenbauer-Kukic for assistance with sample collection.

Authors' roles: Study design: NE, AM, MM, BFZ, SE, VCD, CRF. Study conduct: NE, AM, MM, BFZ, SE, VCD, CRF. Data collection: RK, BN, EM, HB, JX, AB, JJ, NC. Data analysis: NE, KCO, MH, CGJ, JOD, JX, NC, CH, CRF. Data interpretation: NE, KCO, MH, CGJ, JOD, JX, BFZ, CH, UK, SE, VCD, CRF. Drafting manuscript: NE, CRF. Revising manuscript and content: NE, HB, BFZ, UK, SE, VCD, CRF. Approving final version of the manuscript: NE and CRF. NE and CRF take responsibility for the integrity of the data analysis.

NE was supported by the Clinician Scientist Program, funded by the Berlin Institute of Health and the Charité – Universitätsmedizin Berlin, and the Rahel-Hirsch program (Charité). This research was supported in part by the Intramural Research Program of the National Human Genome Research Institute, National Institutes of Health.

8. References

[1]. Catel W, Differentialdiagnose von Krankheitssymptomen bei Kindern und Jugendlichen, 3 ed., Stuttgart: G. Thieme1961.

[2]. Manzke H, [Symmetrical hyperphalangy of the second finger by a supplementary metacarpus bone], Fortschritte auf dem Gebiete der Rontgenstrahlen und der Nuklearmedizin 105(3) (1966) 425–7. [PubMed: 6011685]

[3]. Manzke H, Lehmann K, Klopocki E, Caliebe A, Catel-Manzke syndrome: two new patients and a critical review of the literature, European journal of medical genetics 51(5) (2008) 452–65. [PubMed: 18501694]

[4]. Ehmke N, Caliebe A, Koenig R, Kant SG, Stark Z, Cormier-Daire V, Wieczorek D, Gillessen-Kaesbach G, Hoff K, Kawalia A, Thiele H, Altmuller J, Fischer-Zirnsak B, Knaus A, Zhu N, Heinrich V, Huber C, Harabula I, Spielmann M, Horn D, Kornak U, Hecht J, Krawitz PM, Nurnberg P, Siebert R, Manzke H, Mundlos S, Homozygous and compound-heterozygous mutations in TGDS cause Catel-Manzke syndrome, American journal of human genetics 95(6) (2014) 763–70. [PubMed: 25480037]

[5]. Schoner K, Bald R, Horn D, Rehder H, Kornak U, Ehmke N, Mutations in TGDS associated with additional malformations of the middle fingers and halluces: Atypical Catel-Manzke syndrome in a fetus, American journal of medical genetics. Part A 173(6) (2017) 1694–1697. [PubMed: 28422407]

[6]. Pogue R, Marques FA, Kopacek C, Rosa RCM, Dorfman LE, Mazzeu JF, Flores JAM, Zen PRG, Rosa RFM, Short stature, unusual face, delta phalanx, and abnormal vertebrae and ribs in a girl born to half-siblings, American journal of medical genetics. Part A 173(5) (2017) 1152–1158. [PubMed: 28371255]

[7]. Stanghellini I, Dassi E, Bertorelli R, De Sanctis V, Caleffi A, Landi A, Percesepe A, Exome sequencing in a patient with Catel-Manzke-like syndrome excludes the involvement of the known genes and reveals a possible candidate, European journal of medical genetics 58(11) (2015) 597–602. [PubMed: 26420031]

[8]. Shi H, Enriquez A, Rapadas M, Martin E, Wang R, Moreau J, Lim CK, Szot JO, Ip E, Hughes JN, Sugimoto K, Humphreys DT, McInerney-Leo AM, Leo PJ, Maghzal GJ, Halliday J, Smith J, Colley A, Mark PR, Collins F, Sillence DO, Winlaw DS, Ho JWK, Guillemin GJ, Brown MA, Kikuchi K, Thomas PQ, Stocker R, Giannoulatou E, Chapman G, Duncan EL, Sparrow DB, Dunwoodie SL, NAD Deficiency, Congenital Malformations, and Niacin Supplementation, N Engl J Med 377(6) (2017) 544–552. [PubMed: 28792876]

[9]. Christensen M, Duno M, Lund AM, Skovby F, Christensen E, Xanthurenic aciduria due to a mutation in KYNU encoding kynureninase, J Inherit Metab Dis 30(2) (2007) 248–55. [PubMed: 17334708]

[10]. Li H, Aligning sequence reads, clone sequences and assembly contigs with BWA-MEM., arXiv, arXiv:1303.3997v2 (2013).

[11]. DePristo MA, Banks E, Poplin R, Garimella KV, Maguire JR, Hartl C, Philippakis AA, del Angel G, Rivas MA, Hanna M, McKenna A, Fennell TJ, Kernytsky AM, Sivachenko AY, Cibulskis K, Gabriel SB, Altshuler D, Daly MJ, A framework for variation discovery and genotyping using next-generation DNA sequencing data, Nature genetics 43(5) (2011) 491–8. [PubMed: 21478889]

[12]. Strauss KA, Gonzaga-Jauregui C, Brigatti KW, Williams KB, King AK, Van Hout C, Robinson DL, Young M, Praveen K, Heaps AD, Kuebler M, Baras A, Reid JG, Overton JD, Dewey FE, Jinks RN, Finnegan I, Mellis SJ, Shuldiner AR, Puffenberger EG, Genomic diagnostics within a medically underserved population: efficacy and implications, Genet Med 20(1) (2018) 31–41. [PubMed: 28726809]

[13]. Adzhubei IA, Schmidt S, Peshkin L, Ramensky VE, Gerasimova A, Bork P, Kondrashov AS, Sunyaev SR, A method and server for predicting damaging missense mutations, Nature methods 7(4) (2010) 248–9. [PubMed: 20354512]

[14]. Kumar P, Henikoff S, Ng PC, Predicting the effects of coding non-synonymous variants on protein function using the SIFT algorithm, Nature protocols 4(7) (2009) 1073–81. [PubMed: 19561590]

[15]. Schwarz JM, Rodelsperger C, Schuelke M, Seelow D, MutationTaster evaluates disease-causing potential of sequence alterations, Nature methods 7(8) (2010) 575–6. [PubMed: 20676075]

[16]. Sherry ST, Ward MH, Kholodov M, Baker J, Phan L, Smigielski EM, Sirotkin K, dbSNP: the NCBI database of genetic variation, Nucleic acids research 29(1) (2001) 308–11. [PubMed: 11125122]

[17]. Genomes Project C, Auton A, Brooks LD, Durbin RM, Garrison EP, Kang HM, Korbel JO, Marchini JL, McCarthy S, McVean GA, Abecasis GR, A global reference for human genetic variation, Nature 526(7571) (2015) 68–74. [PubMed: 26432245]

[18]. Lek M, Karczewski KJ, Minikel EV, Samocha KE, Banks E, Fennell T, O'Donnell-Luria AH, Ware JS, Hill AJ, Cummings BB, Tukiainen T, Birnbaum DP, Kosmicki JA, Duncan LE, Estrada K, Zhao F, Zou J, Pierce-Hoffman E, Berghout J, Cooper DN, Deflaux N, DePristo M, Do R, Flannick J, Fromer M, Gauthier L, Goldstein J, Gupta N, Howrigan D, Kiezun A, Kurki MI, Moonshine AL, Natarajan P, Orozco L, Peloso GM, Poplin R, Rivas MA, Ruano-Rubio V, Rose SA, Ruderfer DM, Shakir K, Stenson PD, Stevens C, Thomas BP, Tiao G, Tusie-Luna MT, Weisburd B, Won HH, Yu D, Altshuler DM, Ardissino D, Boehnke M, Danesh J, Donnelly S, Elosua R, Florez JC, Gabriel SB, Getz G, Glatt SJ, Hultman CM, Kathiresan S, Laakso M, McCarroll S, McCarthy MI, McGovern D, McPherson R, Neale BM, Palotie A, Purcell SM, Saleheen D, Scharf JM, Sklar P, Sullivan PF, Tuomilehto J, Tsuang MT, Watkins HC, Wilson JG, Daly MJ, MacArthur DG, Exome Aggregation C, Analysis of protein-coding genetic variation in 60,706 humans, Nature 536(7616) (2016) 285–91. [PubMed: 27535533]

[19]. Faust GG, Hall IM, SAMBLASTER: fast duplicate marking and structural variant read extraction, Bioinformatics 30(17) (2014) 2503–5. [PubMed: 24812344]

[20]. Jager M, Wang K, Bauer S, Smedley D, Krawitz P, Robinson PN, Jannovar: a java library for exome annotation, Human mutation 35(5) (2014) 548–55. [PubMed: 24677618]

[21]. Forbes SA, Beare D, Boutselakis H, Bamford S, Bindal N, Tate J, Cole CG, Ward S, Dawson E, Ponting L, Stefancsik R, Harsha B, Kok CY, Jia M, Jubb H, Sondka Z, Thompson S, De T, Campbell PJ, COSMIC: somatic cancer genetics at high-resolution, Nucleic acids research 45(D1) (2017) D777–D783. [PubMed: 27899578]

[22]. Karczewski KJ, Francioli LC, Tiao G, Cummings BB, Alföldi J, Wang Q, Collins RL, Laricchia KM, Ganna A, Birnbaum DP, Gauthier LD, Brand H, Solomonson M, Watts NA, Rhodes D, Singer-Berk M, Seaby EG, Kosmicki JA, Walters RK, Tashman K, Farjoun Y, Banks E, Poterba T, Wang A, Seed C, Whiffin N, Chong JX, Samocha KE, Pierce-Hoffman E, Zappala Z, O'Donnell-Luria AH, Vallabh Minikel E, Weisburd B, Lek M, Ware JS, Vittal C, Armean IM, Bergelson L, Cibulskis K, Connolly KM, Covarrubias M, Donnelly S, Ferriera S, Gabriel S, Gentry J, Gupta N, Jeandet T, Kaplan D, Llanwarne C, Munshi R, Novod S, Petrillo N, Roazen D, Ruano-Rubio V, Saltzman A, Schleicher M, Soto J, Tibbetts K, Tolonen C, Wade G, Talkowski ME, Neale BM, Daly MJ, MacArthur DG, Variation across 141,456 human exomes

and genomes reveals the spectrum of loss-of-function intolerance across human protein-coding genes, bioRxiv (2019) 531210.

[23]. Pedersen BS, Quinlan AR, Who's Who? Detecting and Resolving Sample Anomalies in Human DNA Sequencing Studies with Peddy, American journal of human genetics 100(3) (2017) 406–413. [PubMed: 28190455]

[24]. Li H, A statistical framework for SNP calling, mutation discovery, association mapping and population genetical parameter estimation from sequencing data, Bioinformatics 27(21) (2011) 2987–93. [PubMed: 21903627]

[25]. Landrum MJ, Lee JM, Benson M, Brown GR, Chao C, Chitipiralla S, Gu B, Hart J, Hoffman D, Jang W, Karapetyan K, Katz K, Liu C, Maddipatla Z, Malheiro A, McDaniel K, Ovetsky M, Riley G, Zhou G, Holmes JB, Kattman BL, Maglott DR, ClinVar: improving access to variant interpretations and supporting evidence, Nucleic acids research 46(D1) (2018) D1062–D1067. [PubMed: 29165669]

[26]. Miller MJ, Kennedy AD, Eckhart AD, Burrage LC, Wulff JE, Miller LA, Milburn MV, Ryals JA, Beaudet AL, Sun Q, Sutton VR, Elsea SH, Untargeted metabolomic analysis for the clinical screening of inborn errors of metabolism, J Inherit Metab Dis 38(6) (2015) 1029–39. [PubMed: 25875217]

[27]. Kennedy AD, Miller MJ, Beebe K, Wulff JE, Evans AM, Miller LA, Sutton VR, Sun Q, Elsea SH, Metabolomic Profiling of Human Urine as a Screen for Multiple Inborn Errors of Metabolism, Genet Test Mol Biomarkers 20(9) (2016) 485–95. [PubMed: 27448163]

[28]. Evans AM, DeHaven CD, Barrett T, Mitchell M, Milgram E, Integrated, nontargeted ultrahigh performance liquid chromatography/electrospray ionization tandem mass spectrometry platform for the identification and relative quantification of the small-molecule complement of biological systems, Anal Chem 81(16) (2009) 6656–67. [PubMed: 19624122]

[29]. Dehaven CD, Evans AM, Dai H, Lawton KA, Organization of GC/MS and LC/MS metabolomics data into chemical libraries, J Cheminform 2(1) (2010) 9. [PubMed: 20955607]

[30]. Rentzsch P, Witten D, Cooper GM, Shendure J, Kircher M, CADD: predicting the deleteriousness of variants throughout the human genome, Nucleic acids research 47(D1) (2019) D886–D894. [PubMed: 30371827]

[31]. Bogan KL, Brenner C, Nicotinic acid, nicotinamide, and nicotinamide riboside: a molecular evaluation of NAD+ precursor vitamins in human nutrition, Annu Rev Nutr 28 (2008) 115–30. [PubMed: 18429699]

[32]. Horwitt MK, Harper AE, Henderson LM, Niacin-tryptophan relationships for evaluating niacin equivalents, Am J Clin Nutr 34(3) (1981) 423–7. [PubMed: 6452053]

[33]. Shibata K, Blood Pyridine Nucleotide Levels Reflect Niacin Equivalent Intake in Humans J Clin Biochem Nutr 3 (1987) 37–45.

[34]. Creeke PI, Dibari F, Cheung E, van den Briel T, Kyroussis E, Seal AJ, Whole blood NAD and NADP concentrations are not depressed in subjects with clinical pellagra, J Nutr 137(9) (2007) 2013–7. [PubMed: 17709435]

[35]. Mankin HJ, Lippiello L, The glycosaminoglycans of normal and arthritic cartilage, J Clin Invest 50(8) (1971) 1712–9. [PubMed: 4255496]

[36]. Moriarity JL, Hurt KJ, Resnick AC, Storm PB, Laroy W, Schnaar RL, Snyder SH, UDP-glucuronate decarboxylase, a key enzyme in proteoglycan synthesis: cloning, characterization, and localization, The Journal of biological chemistry 277(19) (2002) 16968–75. [PubMed: 11877387]

[37]. Li B, Balasubramanian K, Krakow D, Cohn DH, Genes uniquely expressed in human growth plate chondrocytes uncover a distinct regulatory network, BMC Genomics 18(1) (2017) 983. [PubMed: 29262782]

[38]. Ranganath P, Dalal AB, Congenital metacarpal pseudoarthrosis, cleft palate, short stature, advanced bone age, and genu valgum: a new syndrome or a variant of Devriendt syndrome?, Clinical dysmorphology 22(2) (2013) 73–5. [PubMed: 23448907]

[39]. Koenig R, Meinecke P, Fuchs S, A second case of Devriendt syndrome, Clinical dysmorphology 14(1) (2005) 19–22. [PubMed: 15602088]

[40]. Devriendt K, Keymolen K, Roelen L, Van Goethem G, Meireleire J, Fryns JP, Severe short stature, hyperphalangy of the index fingers, mental retardation and facial dysmorphism, Clinical dysmorphology 9(2) (2000) 111–4. [PubMed: 10826622]

[41]. Huber C, Oules B, Bertoli M, Chami M, Fradin M, Alanay Y, Al-Gazali LI, Ausems MG, Bitoun P, Cavalcanti DP, Krebs A, Le Merrer M, Mortier G, Shafeghati Y, Superti-Furga A, Robertson SP, Le Goff C, Muda AO, Paterlini-Brechot P, Munnich A, Cormier-Daire V, Identification of CANT1 mutations in Desbuquois dysplasia, American journal of human genetics 85(5) (2009) 706–10. [PubMed: 19853239]

[42]. Gotting C, Muller S, Schottler M, Schon S, Prante C, Brinkmann T, Kuhn J, Kleesiek K, Analysis of the DXD motifs in human xylosyltransferase I required for enzyme activity, The Journal of biological chemistry 279(41) (2004) 42566–73. [PubMed: 15294915]

[43]. Muller S, Schottler M, Schon S, Prante C, Brinkmann T, Kuhn J, Gotting C, Kleesiek K, Human xylosyltransferase I: functional and biochemical characterization of cysteine residues required for enzymic activity, Biochem J 386(Pt 2) (2005) 227–36. [PubMed: 15461586]

[44]. Casanova JC, Kuhn J, Kleesiek K, Gotting C, Heterologous expression and biochemical characterization of soluble human xylosyltransferase II, Biochem Biophys Res Commun 365(4) (2008) 678–84. [PubMed: 18023272]

[45]. Khatra BS, Herries DG, Brew K, Some kinetic properties of human-milk galactosyl transferase, Eur J Biochem 44(2) (1974) 537–60. [PubMed: 4209349]

[46]. Yokota H, Ando F, Iwano H, Yuasa A, Inhibitory effects of uridine diphosphate on UDP-glucuronosyltransferase, Life Sci 63(19) (1998) 1693–9. [PubMed: 9806225]

[47]. Rens-Domiano SS, Roth JA, Inhibition of M and P phenol sulfotransferase by analogues of 3'-phosphoadenosine-5'-phosphosulfate, J Neurochem 48(5) (1987) 1411–5. [PubMed: 3470439]

[48]. Balasubramanian M, Lord H, Levesque S, Guturu H, Thuriot F, Sillon G, Wenger AM, Sureka DL, Lester T, Johnson DS, Bowen J, Calhoun AR, Viskochil DH, Study DDD, Bejerano G, Bernstein JA, Chitayat D, Chitayat syndrome: hyperphalangism, characteristic facies, hallux valgus and bronchomalacia results from a recurrent c.266A>G p.(Tyr89Cys) variant in the ERF gene, Journal of medical genetics 54(3) (2017) 157–165. [PubMed: 27738187]

[49]. Schwabe GC, Turkmen S, Leschik G, Palanduz S, Stover B, Goecke TO, Mundlos S, Brachydactyly type C caused by a homozygous missense mutation in the prodomain of CDMP1, American journal of medical genetics. Part A 124A(4) (2004) 356–63. [PubMed: 14735582]

Highlights

- We describe a new genetic etiology of Catel-Manzke syndrome.
- Multisystemic features other than hyperphalangism include spine, heart, renal, and inner ear malformations.
- Detection of xanthurenic aciduria on biochemical testing can aid in the differential diagnosis of hyperphalangism.

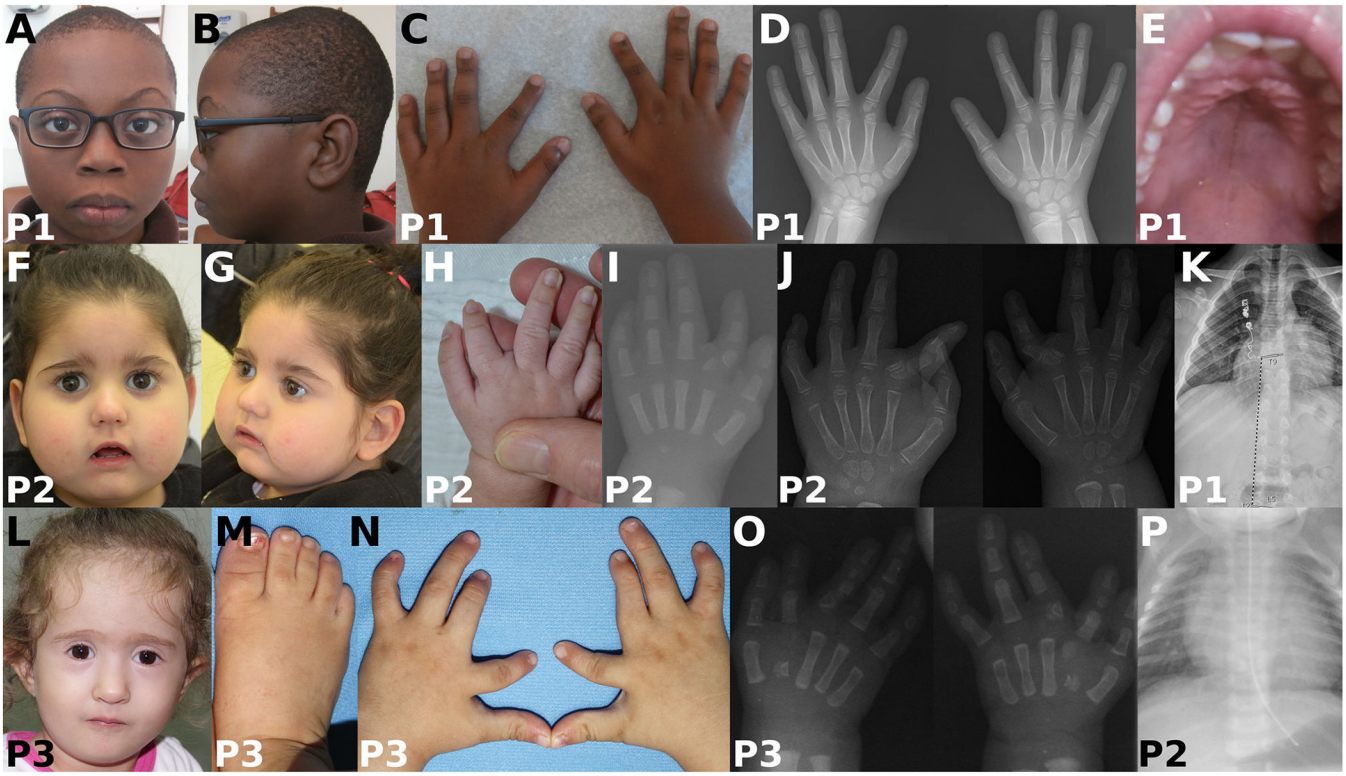

Figure 1. Clinical pictures and radiographs of patients 1–3 showing the clinical features of kyruneninase deficiency with hyperphalangism.

(A, B, E) Clinical photographs of Patient 1, showing microretrognathia, highly arched eyebrows and a high palate. **(C, D)** Photographs and radiographs of the hands of Patient 1. Note the bilateral radial deviation and mild ulnar clinodactyly of the index fingers, due to supernumerary epiphyseal centers at the base of the second proximal phalanges. Photo and radiograph obtained at the age of 10 years. **(F, G)** Facial photographs of Patient 2. Note narrow forehead, low anterior hairline, full cheeks, and normal chin. **(H, I, J)** Photographs and radiographs of the hands of Patient 2. Note shortening and radial deviation of the index fingers, due to an accessory ossicle at the base of the second proximal phalanges. The secondary ossification centers represent longitudinally bracketed epiphyses (delta phalanges). Radiographs were taken at the age of 5 weeks (I) and 4 years (J). **(K)** Radiographs of the spine of Patient 1. Note butterfly vertebrae at T10-T11 (red arrow) and scoliosis. **(L)** Facial photographs of Patient 3. Note a high anterior hairline, narrow mouth with downturned corners, thin vermilion of the upper and lower lips, and protruding ears. **(M)** Photograph of the right foot of Patient 3. Note partial cutaneous syndactyly of toes 2 and 3 and small fifth toe nails. **(N)** Hand photographs of Patient 3 at the age of 5 years. Note shortening, radial deviation and ulnar clinodactyly of the index fingers, short middle fingers with ulnar deviation, and clinodactyly of the fifth fingers. **(O)** Hand radiographs of Patient 3 at the age of 5 years. Note bilateral supernumerary epiphyseal centers at the ulnar side of the base of the second proximal phalanges and at the radial side of the base of the third proximal phalanges with consequent shortening of third proximal phalanges, severe hypoplasia of the second metacarpals with longitudinally bracketed epiphyses, and hypoplasia of the middle

phalanges of the index, third and fifth fingers. **(P)** Radiographs of the spine of Patient 2. Note butterfly vertebrae at T8 (red arrow).

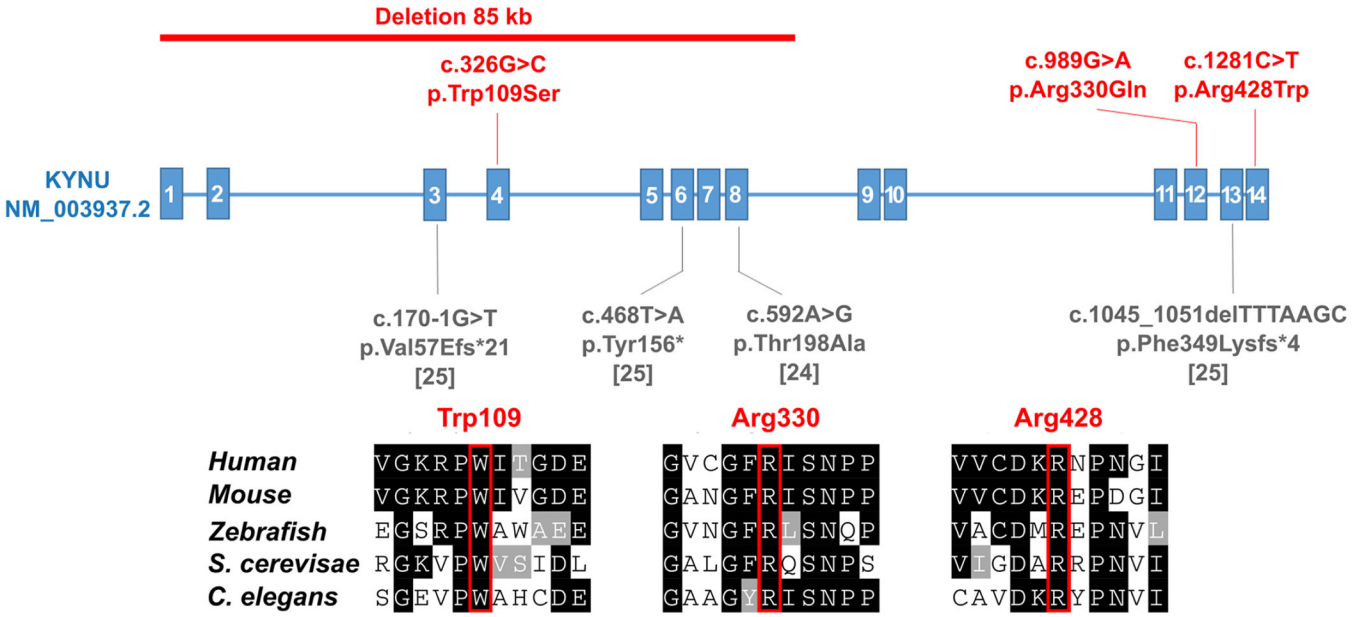

Figure 2. Novel and previously reported human *KYNU* mutations.

Scheme of *KYNU* indicating the position of the detected mutations (above) compared to the previously reported mutations (below), and the conservation of the affected amino acid positions for the novel variants.

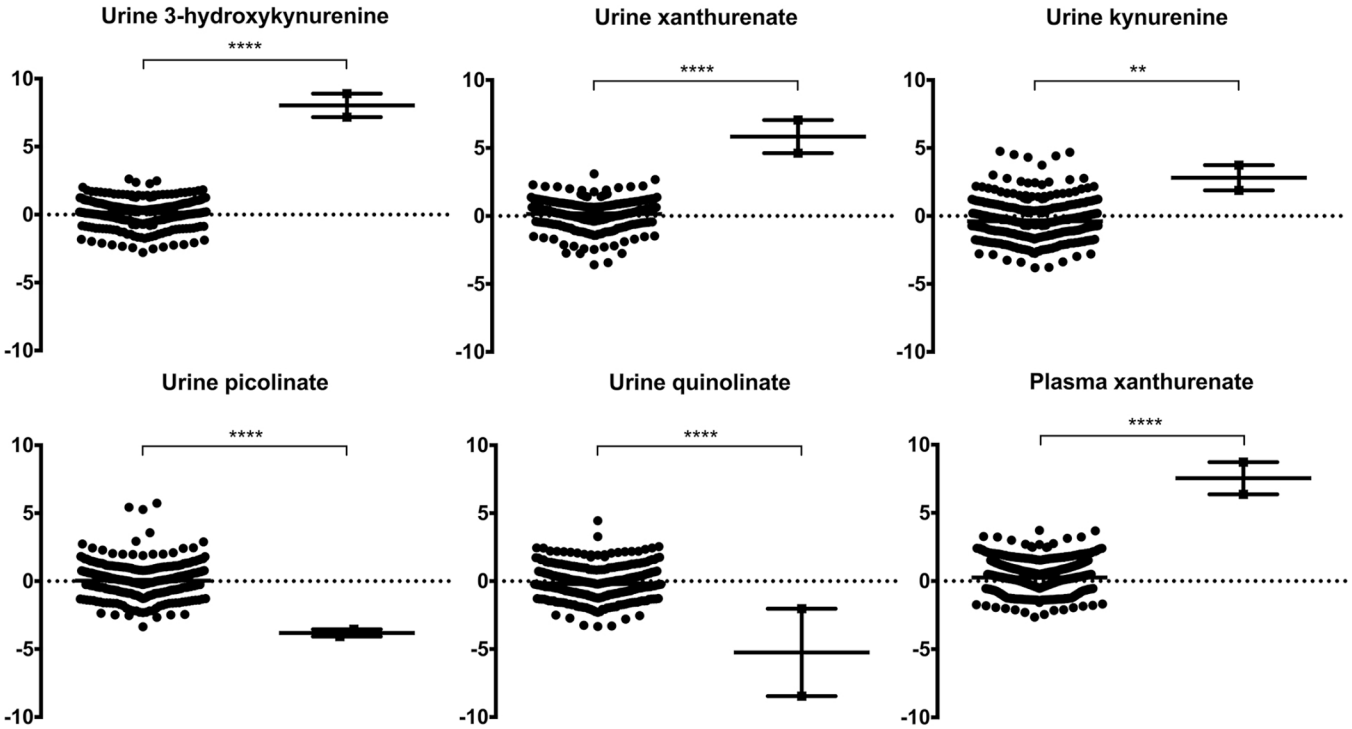

Figure 3. Metabolites in the tryptophan degradation pathway.

Metabolomic profiling revealed a statistically significant elevation in metabolites proximal to the block (3-hydroxykynurenine, xanthurenate, kynurenine) with concomitantly decreased metabolites distal to the block (picolinate, quinolinate). ****, $p<0.0001$; **, $p<0.01$.

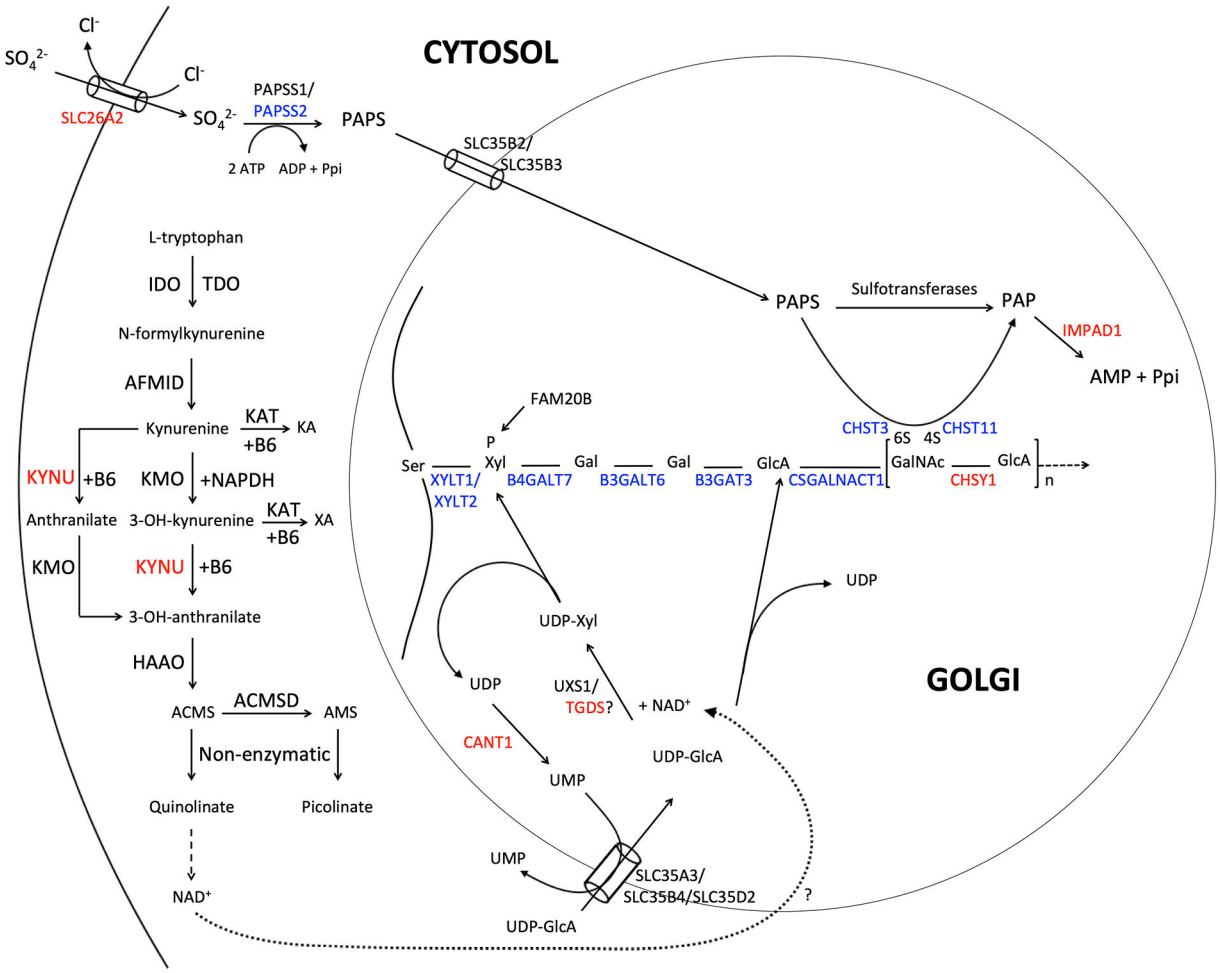

Figure 4. Hypothetical mechanism of hyperphalangism in the setting of kynureninase deficiency.

Names in red indicate enzyme deficiencies associated with hyperphalangism or delta-shaped phalanges, while names in blue indicate enzyme deficiencies associated with other skeletal involvement. Mutations in *CANT1* are associated with Desbuquois dysplasia type 1 [41] and consequent hyperphalangism of the index fingers. *CANT1* encodes a nucleotidase, the deficiency of which leads to accumulation of UDP, a known inhibitor of multiple glycosyltransferases, in particular those that transfer xylose [42–44], galactose [45], and glucuronic acid [46]. *IMPAD1* encodes the Golgi-resident PAP-specific 3'-phosphatase (gPAPP), the deficiency of which leads to accumulation of PAP, a known inhibitor of sulfotransferases [41, 47]. gPAPP deficiency is associated with variable hyperphalangism. Mutations in *CHSY1*, encoding the chondroitin sulfate synthase, are associated with hyperphalangism of digits 1–3 [41]. Note that mutations in the genes encoding the transcription factors *ERF* and *GDF5* also lead to hyperphalangism [48, 49].

Table 1.

Clinical and molecular features of *KYNU/HAAO*-associated malformation syndromes compared to TGDS-associated Catel-Manzke syndrome.

	This study			Patients with *KYNU* and *HAAO* LOF variants (Shi *et al.* 2017)	*TGDS*-associated Catel-Manzke syndrome (Ehmke *et al.* 2014, Pferdehirt *et al.* 2015, Schoner *et al.* 2017)
	Patient 1	**Patient 2**	**Patient 3**		
Sex	Male	Female	Female	3 female/1 male	6 female/3 male
Ethnicity	Caribbean	Turkish	Turkish	Diverse	Diverse
Consanguinity	–	+	+	3/4	–
Age at last exam	13 y 6 m	3 y	5 y	4 m-12 y	na
***KYNU* mutations (NM_003937.2)**					
1st mutation	delEx1–8	c.989G>A; p.Arg330Gln	c.326G>C; p.Trp109Ser	LOF variants	na
2nd mutation	c.1282C>T; p.Arg428T rp	c.989G>A; p.Arg330Gln	c.326G>C; p.Trp109Ser	–	na
Type	Compound heterozygous	Homozygous	Homozygous	Biallelic	na
Clinical manifestations					
Short stature (HP:0004322)	−2.3 SD	−4.6 SD	−2.2 SD	2/4	2/9 (postnatal)
Vertebral anomalies (HP:0003468)	Butterfly vertebrae T10–11, scoliosis	Butterfly vertebra T8	–	4/4 (segmentation defects)	1/9 (scoliosis)
Talipes (HP:0001883)	–	–	–	2/4	1/9
Manzke dysostosis/Finger hyperphalangism (HP:0009495/ HP:0030367)	+	+	+	nr	9/9
Other limb defects (HP:0040068)	–	Long thumbs	Short 3rd fingers and short 2nd metacarpals due to accessory ossicles, clinodactyly of 5th fingers, 2,3-toe syndactyly,	3/4 (2,3-toe syndactyly, rhizomelia, short long bones)	2/9: short long bones; 1/9: 11 pairs of ribs 1/9: short 3rd fingers 3/9 clinodactyly of 5th fingers
Pierre Robin sequence with cleft palate (HP:0000201)	–	–	–	1/4 (cleft palate)	7/9
Microretrognathia (HP:0000308)	+	–	+	nr	2/9
Renal malformation (HP:0012210)	–	–	Unilateral renal agenesis	4/4	0/9
Congenital heart defect (HP:0001627)	Hypoplastic left heart	Tetralogy of Fallot, ALCAPA	Secundum ASD, subaortic VSD	4/4	4/9
Developmental delay (HP 0001263)	Mild	+	Mild	2/4	0/8

	This study			Patients with *KYNU* and *HAAO* LOF variants (Shi *et al.* 2017)	*TGDS*-associated Catel-Manzke syndrome (Ehmke *et al.* 2014, Pferdehirt *et al.* 2015, Schoner *et al.* 2017)
	Patient 1	**Patient 2**	**Patient 3**		
Muscular hypotonia (HP:0001252)	−	Severe	−	nr	nr
Failure to thrive (HP:0001531)	−	+, PEG feeding	−	1/4	1/8
Microcephaly	−	−6.4 SD	−2.3 SD	2/4	0/9
Facial dysmorphism (HP:0001999)	+	+	+	2/4	7/9 (nr in 2/9)
Joint hypermobility (HP:0001382)	−	−	+	nr	2/8 (nr in 6/8)
Premature death	na	na	na	2/4	1/9 (interruption of pregnancy)
Sensorineural hearing loss (HP:0000407)	nr	+	nr	2/4	1/8
Malformation of cochlea and semicircular canals (HP:0008554, HP:0011380)	nr	+	nr	1/4	nr
Other	Hepatomegaly	−	Bilateral single transverse palmar crease	Anterior anus 1/4; short neck 1/4; hypothyroidism1/4, laryngomalacia 1/4	1/9: short neck 2/9: pectus deformity 1/9: laryngo- and pharyngomalacia

Abbreviations: y, year; m, month; nr, not reported; na, not applicable; ALCAP, anomalous origin of the left coronary artery from the pulmonary artery; ASD, atrial septal defect; PEG, percutaneous endoscopic gastrostomy; SD, standard deviation; VSD, ventricular septal defect.

Table 2.

Metabolite concentrations in patients compared to a control population. Bolded numbers indicate significant p-values. SEM, standard error of the mean.

Metabolite	Z-score							p-value
	Controls			Patients (n = 2)				
	N	Mean	SEM	Patient 1	Patient 2	Mean	SEM	
Urine								
3-hydroxykynurenine	375	0.16	0.05	8.89	7.17	8.03	0.86	**<0.0001**
Xanthurenate	344	0.14	0.97	7.06	4.62	5.84	1.21	**<0.0001**
Kynurenine	387	−0.39	0.07	3.74	1.88	2.8	0.93	**0.0013**
Kynurenate	387	−0.04	0.04	0.61	−1.19	−0.29	0.90	0.7055
3-hydroxyanthranilate	375	0.16	0.05	−1.47	−1.27	−1.37	0.10	**0.0187**
Anthranilate	272	0.23	0.08	−2.35	−0.31	−1.33	1.01	0.1047
Picolinate	387	0.04	0.06	−4.08	−3.55	−3.81	0.27	**<0.0001**
Quinolinate	387	−0.16	0.06	−8.46	−2.03	−5.25	3.22	**<0.0001**
Tryptophan	387	0.11	0.05	−0.43	−2.38	−1.4	0.97	0.0351
Plasma								
Xanthurenate	1,437	0.26	0.03	8.72	6.36	7.54	1.18	**<0.0001**
Kynurenate	2,083	0.12	0.03	3.47	−0.21	1.63	1.84	0.0945
Kynurenine	2,087	0.11	0.025	1.09	1.58	1.33	0.24	0.1304
Tryptophan	2,087	−0.13	0.026	1.50	0.11	0.80	0.98	0.2657